

Statistical Mechanics of Dense Ionized Matter. II. Equilibrium Properties and Melting Transition of the Crystallized One-Component Plasma

E. L. Pollock* and J. P. Hansen†

Laboratoire de Physique Théorique et Hautes Energies, Orsay, France

(Received 13 April 1973)

A study of the crystalline phase of a one-component plasma in a uniform background is reported here. Extensive Monte Carlo computations of the equilibrium properties in the classical region are presented and a value of the melting parameter $\Gamma_m = 155 \pm 10$ is obtained. These results are extended into the quantum region in the framework of conventional lattice dynamics to estimate the solid-fluid coexistence curve in conjunction with the Lindemann melting criterion. A preliminary investigation is made of the effect of allowing the charge neutralizing background to respond to the ionic motion and it is concluded that the melting curve will be unaffected for ions with $Z \geq 2$.

I. INTRODUCTION

In the first paper of this series¹ (hereafter referred to as I), the equilibrium properties of the classical one-component plasma (ocp) in a uniform background of opposite charge were calculated by the Monte Carlo method of Metropolis *et al.*² An equation of state for the fluid phase of the ocp was derived from which all other thermodynamic properties can be obtained. The first aim of the present paper is to extend these computations to higher densities, where we expect a solid phase to appear, and to determine the fluid-solid coexistence curve with reasonable accuracy. The importance of this transition in the study of dense stellar matter (e.g., white-dwarf interiors) has been stressed many times, but only semiquantitative estimates of the transition line appeared until now in the literature.^{3,4}

The second purpose of this paper is the extension of the ocp model in two directions. A first extension is the inclusion of quantum effects in the crystalline phase. Because a finite-temperature Monte Carlo scheme for the study of quantum many-body systems is still lacking, we use lattice dynamics in that part of the work. This allows us to present a refined version of the recent calculation by Hansen, Jancovici, and Schiff⁵ of the phase diagram of the ocp in a uniform background, assuming the validity of Lindemann's melting criterion. The second extension is the replacement of the uniform background by a responsive one. This is achieved by allowing dielectric screening by the background, i.e., by replacing a constant dielectric function by a wave-number-dependent one. The main result of that part of our work is that the phase diagram obtained previously for a system of completely ionized atoms is rather insensitive to the inclusion of dielectric screening for all values of Z , the atomic number of the nuclei,

except $Z = 1$ (H and D nuclei).

We briefly recall here that the excess thermodynamic properties of a classical system of N particles interacting by the repulsive Coulomb potential,

$$u(r) = (Ze)^2/r,$$

and immersed in a uniform background of opposite charge, depend only on the dimensionless parameter

$$\Gamma = (Ze)^2/kT\bar{r},$$

where \bar{r} is the ion-sphere (or Wigner-Seitz) radius

$$\bar{r} = \left(\frac{3}{4\pi\rho} \right)^{1/3},$$

ρ is the number density N/V , and V is the total volume of the system. We shall also use the dimensionless ion-sphere radius $r_s = \bar{r}/a$, where a is the ionic Bohr radius.

The outline of the paper is the following. In Sec. II, the Monte Carlo results obtained for systems of $N = 16, 54, 128$, and 250 ions are presented in the range $140 \leq \Gamma \leq 300$. The deviations of the computed root-mean-square (rms) displacement of the ions and of the internal energy, from the predictions of harmonic lattice dynamics, are investigated. From these considerations a simple equation of state of the crystalline ocp is derived, and the Helmholtz free energy is calculated as a function of Γ .

In Sec. III a comparison of these free-energy data, with the free energy of the fluid, taken from I, allows us to locate the fluid-solid phase transition.

The extension to the quantum regime is presented in Sec. IV, in the framework of lattice dynamics. The coexistence curve is determined over the whole ρ - T plane, in the spirit of the re-

cent work by Hansen *et al.*⁵

Section V is devoted to the introduction of dielectric screening of the background. Modifications of the lattice-dynamics results due to dielectric screening are analyzed and the effect of the screening on the coexistence curve is shown to be small for most values of the atomic number Z of the ions.

Some concluding remarks and indications of future work are contained in Sec. VI.

Parts of this work were briefly reported elsewhere.⁶

II. MONTE CARLO COMPUTATIONS OF EQUILIBRIUM PROPERTIES

Consider a system of N ions in a cubic box of edge length L . If the interionic distance r is expressed in units of \bar{r} , the pair potential divided by kT reads

$$u(r)/kT = \Gamma/r. \quad (2.1)$$

Assuming periodic boundary conditions, we replace, following Brush, Sahlin, and Teller,³ the "bare" Coulomb potential (1) by an effective "Ewald potential" which takes into account all the periodic images of the ions contained in the initial box, as well as the interaction of the ions with the uniform background. This Ewald potential, divided by kT , can be set in the form^{1,3}

$$\Gamma v(\bar{r}) = \frac{\Gamma}{L} \left(\sum_{\bar{\lambda}} \frac{\operatorname{erfc}[\pi^{1/2} |(\bar{r}/L) + \bar{\lambda}|]}{|(\bar{r}/L) + \bar{\lambda}|} - 1 + \sum_{\bar{\lambda}}' \frac{e^{-\pi^2 \bar{\lambda}^2}}{\pi \bar{\lambda}^2} e^{2i\pi \bar{\lambda} \cdot (\bar{r}/L)} \right). \quad (2.2)$$

The sums go over all vectors $\bar{\lambda}$ with integer coordinates; the primed sum means that the term $\bar{\lambda} = (0, 0, 0)$ is omitted; $\operatorname{erfc}(x)$ denotes the usual error-function complement. We refer the reader to I for a derivation of (2.2) as well as for some technical details concerning the approximation of the Ewald potential by an "optimized" expansion in Kubic harmonics⁷ in the Monte Carlo programs.

Properties of the solid phase were investigated by Monte Carlo simulations in the range $140 \leq \Gamma \leq 300$. The initial configuration in each run was taken to be a perfect bcc lattice configuration. Our first aim was to find out below which value of Γ the solid becomes unstable, i.e., melts spontaneously. This was done by inspecting the variation of the mean square displacement of the ions from their original lattice positions, with the number of generated configurations. The computed quantity is the ratio

$$\gamma^2 = \frac{\Delta r^2}{d^2} = \frac{1}{N} \left\langle \sum_i \frac{(\bar{r}_i - \bar{R}_i)^2}{d^2} \right\rangle, \quad (2.3)$$

where d denotes the nearest-neighbor distance in the bcc lattice [$d = (3\pi^2)^{1/3} r_s$], the $\bar{r}_i (i=1, \dots, N)$ are the instantaneous positions, and the \bar{R}_i are the equilibrium positions of the N ions.

For $\Gamma \geq 160$, γ^2 rapidly stabilizes and fluctuates around an average value which depends on the size of the system; the N dependence of γ^2 will be discussed below. The same behavior is still observed for $\Gamma = 150$ with the 128- and 250-particle systems. At the same value of Γ , however, γ^2 increases indefinitely with the number of generated configurations for the two smaller systems, i.e., $N = 16$ and 54. In these cases inspection of the instantaneous positions of all the ions at regular intervals clearly indicates that an increasing number of neighboring particles have exchanged their equilibrium positions as the number of generated configurations increases. This behavior can be interpreted as a first indication of imminent melting. A similar behavior is observed at $\Gamma = 140$ for $N = 128$; below $\Gamma = 135$, the initially crystalline system is always observed to slowly melt, whatever its size. $\Gamma = 135$ can thus be regarded as a lower bound to the value of Γ at melting. It appears from these preliminary results that the solid phase of the larger systems is stable (or metastable) down to slightly lower values of Γ than the smaller systems. This is probably a consequence of the larger rms displacements of the ions in the *smaller* systems, as will be discussed below.

In the range $150 \leq \Gamma \leq 300$, we have computed the excess internal energy per ion, divided by kT , U/NkT , and the rms displacement of the ions around their equilibrium positions, divided by the nearest-neighbor distance γ [see formula (2.3)]. In I it was pointed out that the purely

TABLE I. Excess energy per particle, divided by kT , U/NkT , thermal fraction of that energy $\Delta U/NkT$, excess specific heat per particle C_v/Nk , and rms displacement, divided by the nearest-neighbor distance γ , as a function of Γ for the 128-particle system. The last two columns list the corresponding harmonic values of γ (γ^{harm}) and their infinite-system harmonic values ($\gamma_{\infty}^{\text{harm}}$).

Γ	$\frac{U}{NkT}$	$\frac{\Delta U}{NkT}$	$\frac{C_v}{Nk}$	γ	γ^{harm}	$\gamma_{\infty}^{\text{harm}}$
150	-132.734	1.658	1.98	0.176	0.1766	0.1673
160	-141.717	1.635	1.92	0.168	0.1711	0.1620
170	-150.696	1.616	1.87	0.165	0.1658	0.1571
180	-159.662	1.608	1.83	0.156	0.1612	0.1526
200	-177.604	1.586	1.77	0.146	0.1529	0.1449
220	-195.538	1.572	1.72	0.141	0.1459	0.1378
240	-213.47	1.56	1.69	0.134	0.1396	0.1323
270	-240.354	1.552	1.65	0.124	0.1304	0.1247
300	-267.242	1.544	1.62	0.12	0.1249	0.1183

TABLE II. Thermal fraction of the excess energy per particle, divided by kT , $\Delta U/NkT$, γ [formula (2.3)], and the harmonic value of γ [formula (4.11)], at $\Gamma=200$, for systems of 16, 54, 128, and 250 ions. For $N=128$, we list the Monte Carlo values obtained with four and five Kubic harmonics (KH) approximations of the Ewald potential.

	$N=16$	$N=54$	$N=128$ (4KH)	$N=128$ (5KH)	$N=250$
$\frac{\Delta U}{NkT}$	1.93	1.79	1.571	1.586	1.58
γ	0.169	0.157	0.140	0.146	0.137
γ^{harm}	0.190	0.161	0.153	0.153	0.150

static energy U_0/NkT , i.e., the energy calculated for a perfect lattice configuration, represents a very large fraction of the total energy in the fluid phase for large values of Γ . This is, not surprisingly, even more true in the solid phase, and the thermal fraction of the excess energy $\Delta U/NkT$, i.e., the deviation of the potential energy from its static value due to the thermal motion of the particles, accounts for only about 1% of the total energy. The prediction of harmonic lattice dynamics for the excess internal energy is

$$\frac{U^{\text{harm}}}{NkT} = \frac{U_0}{NkT} + \frac{3}{2} = -0.895\,929\Gamma + \frac{3}{2}. \quad (2.4)$$

Thus harmonic theory predicts a constant value of $\Delta U/NkT$, $\frac{1}{2}$ per degree of freedom. In Table I we list the Monte Carlo values for U/NkT , $\Delta U/NkT$, and γ together with the value of γ from harmonic theory for the 128-particle system; in the Monte Carlo runs the Ewald potential has been approximated by an optimized expansion including five Kubic harmonics. As in I, the $\Delta U/NkT$ data have been corrected for center-of-mass motion by multiplying the Monte Carlo values by $N/(N-1)$. The relative error in $\Delta U/NkT$ is estimated to be of the order of 1%. Inspection of the tabulated data shows that the deviation of $\Delta U/NkT$ from its harmonic value $\frac{3}{2}$ is everywhere of the order of, or less than 10%, and decreases with increasing Γ , as expected. It should be noted, however, that, contrary to the results obtained for other inverse-power potentials, e.g., $1/r^{12}$,^{8,9} the deviation is *positive*. This point will be discussed below.

Table I, moreover, shows that the Monte Carlo values of γ are everywhere close to their harmonic counterparts.

In Table II we list the Monte Carlo values of $\Delta U/NkT$ and γ for $\Gamma=200$ and $N=16, 54, 128$, and 250, using the four Kubic harmonics approximation of the Ewald potential; the table also contains the harmonic values of γ (see Sec. IV) as well as the data obtained with the 128-particle system, if the more accurate approximation of the Ewald

potential, including five Kubic harmonics, is used. The table clearly illustrates that the N dependence of γ is in good agreement with the harmonic predictions; i.e., γ decreases as N increases. Our data at other values of Γ show the same decrease of γ with increasing N . This behavior is the opposite of what has been observed in a hard-sphere solid,¹⁰ where γ decreases with the size of the system.

Table II further shows that the values of $\Delta U/NkT$ are in good agreement for $N=128$ and 250, and differ appreciably only for the smaller systems; this behavior is confirmed by computations at different values of Γ . The difference between $\Delta U/NkT$ calculated with four and five Kubic harmonics to approximate the Ewald potential is within statistical errors.

If one considers the anharmonic contributions to the potential energy as a perturbation, straightforward thermodynamic perturbation theory,¹¹ with the harmonic solid as a reference system, shows that the two leading correction terms to $\Delta U/NkT$ must be proportional to $1/\Gamma$ and $1/\Gamma^2$ or, equivalently, to T and T^2 . Our ocp results, however, strongly suggest that the term proportional to $1/\Gamma$ is very small, possibly identically zero. A least-squares fit to $\Delta U/NkT$ of the form

$$\Delta U/NkT = \frac{3}{2} + \alpha/\Gamma + \beta/\Gamma^2$$

leads to $\alpha \approx 0$, $\beta \approx 3500$.

Moreover, in the framework of the anharmonic cell model, α turns out to be identically 0 in the Coulomb case; this is not true for other power-law potentials, as discussed in the Appendix. The anharmonic corrections calculated for the simple cell model are too small, but have the right sign, i.e., a *negative* correction proportional to T in the case of the $1/r^{12}$, in agreement with the Monte Carlo data of Hoover *et al.*,⁹ and a *positive* correction, proportional to T^2 (or $1/\Gamma^2$) in the case of the Coulomb potential, in agreement with our Monte Carlo data. Thus we have strong reasons to believe that the $1/\Gamma$ correction vanishes and the Monte Carlo data for the excess internal energy are well represented by the formula

$$U/NkT = -0.895\,929\Gamma + 1.5 + 3500/\Gamma^2. \quad (2.5)$$

The equation of state then reads

$$\frac{PV}{NkT} = 1 + \frac{1}{3} \left(\frac{U}{NkT} \right) = -0.298\,643\Gamma + 1.5 + \frac{1167}{\Gamma^2}, \quad (2.6)$$

and the excess specific heat per particle at constant volume is

$$c_v/Nk = 1.5 + 105\,00/\Gamma^2. \quad (2.7)$$

The Helmholtz free energy is obtained by assum-

ing that in the limit $\Gamma \rightarrow \infty$ the harmonic approximation becomes exact. In the classical limit, and for large N , the harmonic approximation yields (see Sec. IV)

$$\frac{F^{\text{harm}}}{NkT} = \frac{F_0}{NkT} + \frac{1}{N} \sum_{j=1}^{3N-3} \ln \frac{\omega}{\omega_p} + 3 \ln \frac{\hbar \omega_p}{kT}, \quad (2.8)$$

where F_0 denotes the purely static contribution, ω_p is the plasma frequency

$$\omega_p = \left(\frac{4\pi(Ze)^2 \rho}{M} \right)^{1/2}, \quad (2.9)$$

M being the mass of the ions, and the sum in (2.8) goes over the $3N-3$ normal modes of the crystal. We have computed the sum as a function of the number of degrees of freedom and find that it tends, in the limit $N \rightarrow \infty$, towards the value -2.4938 ; in the infinite-system limit (see Table III) (2.8) can be rewritten as

$$\begin{aligned} F^{\text{harm}}/NkT = & -0.895929\Gamma - 2.4938 + \frac{3}{2} \ln \frac{3}{2} \\ & + \frac{9}{2} \ln \Gamma + \frac{3}{2} \ln(kT)_{\text{Ry}}. \end{aligned} \quad (2.10)$$

In the last term, the energy kT is expressed in units of ionic rydbergs.

The anharmonic contribution to the free energy is obtained by integrating the anharmonic part of the internal energy (2.5) from $\Gamma = \infty$ to any finite value of Γ . The resulting total Helmholtz free energy is

$$\begin{aligned} F/NkT = & (F^{\text{harm}}/NkT) - 1750/\Gamma^2 \\ = & -0.895929\Gamma + \frac{9}{2} \ln \Gamma - 1.8856 \\ & + \frac{3}{2} \ln(kT)_{\text{Ry}} - 1750/\Gamma^2. \end{aligned} \quad (2.11)$$

III. FLUID-SOLID TRANSITION OF CLASSICAL ONE-COMPONENT PLASMA

Having calculated the free energy as a function of Γ , we are now in a position to locate the fluid-solid phase transition by comparing the free energy of the solid calculated from (2.11) with the free energy of the fluid calculated from formula (22) of I. The two free-energy curves are found to intersect at $\Gamma = 158$ and the solid has the lower free energy for $\Gamma > 158$, whereas the fluid has the lower free energy for $\Gamma < 158$. This value of Γ is somewhat larger than the estimate $\Gamma = 143$ given in the preliminary version of this work⁶ in which the $1/\Gamma^2$ behavior of the anharmonic contribution to the free energy had not yet been established. The free-energy curves of the fluid and solid phases lie very close over a large range of Γ 's, and a 0.1% error in the free energy of one phase shifts the intersection by as much as 15 in Γ ! This illustrates the necessity of very precise Monte Carlo calculations if the fluid-solid transition is

to be determined with a reasonable degree of accuracy.

In the previous section we showed that anharmonicities lower the Helmholtz free energy of the ocp solid. For that reason the intersection of the fluid free-energy curve with the harmonic free-energy curve of the solid (2.10) yields an upper bound to the value of Γ at melting; this intersection occurs at $\Gamma = 170$. Close inspection of our estimated errors on the fluid and solid free energies leads to the estimation $\Gamma = 155 \pm 10$ at melting.

Our upper bound $\Gamma = 170$ lies close to the melting value of Γ predicted by Van Horn,⁴ which is based on the Lindemann criterion in conjunction with harmonic theory and empirical alkali-metal data. The estimate of Brush, Sahlin, and Teller,³ $\Gamma \approx 125$, lies well below our value, in a region where the solid is clearly unstable.

The melting line in the $\rho - T$ plane is now given by

$$T = \chi \rho^{1/3}, \quad (3.1)$$

where

$$\chi = (Ze)^2 \left(\frac{4}{3} \pi \right)^{1/3} / 158k.$$

As is well known,^{1,12} the one-component plasma is unstable (negative pressures and compressibilities) if one does not take into account the free energy of the uniform background. If one chooses the ocp to be a model for dense ionized matter, the background is a degenerate electron gas. If the free energy of the background is added to the free energy of the ions, the intersection point of the free-energy curves of the two phases does not change, but the "width" of the transition, i.e., the relative volume change on melting, $\delta v/v$, determined by a standard Maxwell double-tangent con-

TABLE III. Number dependence of some properties of the bcc solid phase ocp with uniform background in the harmonic approximation. N is the number of particles in the periodically repeated crystal. The moments u_n are defined in Eq. (4.5) of the text, and the last column contains the values of $\ln[\omega_j(\vec{k})/\omega_p]$ averaged over the Brillouin zone. This quantity appears in the classical limit of the lattice free energy [Eq. (4.6)].

N	U_{-2}	U_{-1}	U_1	$\langle \ln \omega \rangle$
8	19.6841	3.5533	0.48446	-2.9460
64	15.4932	3.0138	0.50958	-2.5691
216	14.0733	2.8753	0.51131	-2.5111
512	13.5210	2.8311	0.51148	-2.4982
1000	13.2819	2.8147	0.51147	-2.4949
2744	13.1068	2.8042	0.51143	-2.4937
4096	13.0720	2.8024	0.51142	-2.4936
13824	13.0189	2.7999	0.51140	-2.4937
46656	12.9984	2.7990	0.51139	-2.4938

struction, depends on the exact nature of the background. If the background is a nonrelativistic degenerate electron gas, its free energy is

$$\frac{F^e}{NkT} = \left(\frac{3}{5kT}\right) \frac{\hbar^2}{2m} (3\pi^2 n)^{2/3},$$

where n is the electron number density, $n = Z\rho$. kT will henceforth be expressed in ionic rydbergs; Eq. (3.2) can then be rewritten as

$$\frac{F^e}{NkT} = 1008A Z^{2/3} \Gamma^2 (kT)_{\text{Ry}}, \quad (3.2)$$

where A is the atomic mass of the ions. Formula (3.2) is valid if kT is much smaller than kT_F , where T_F is the Fermi temperature of the electrons. In dimensionless units this condition can be rewritten as

$$(kT)_{\text{Ry}} \ll \frac{2}{3} \frac{Z^{2/3} A 10^4}{r_s^2}$$

or

$$(kT)_{\text{Ry}} \gg \frac{6 \times 10^{-4}}{Z^{2/3} A \Gamma^2}. \quad (3.3)$$

On the other hand, the $\rho - T$ conditions (or, alternatively, the $\Gamma - T$ conditions) must be such that the ions can be considered as classical. In I it was shown that the first quantum correction to the free energy is

$$\frac{F^1}{NkT} = \frac{\Gamma^3 (kT)_{\text{Ry}}}{16}. \quad (3.4)$$

This correction is the same for both phases, at a given value of Γ , which means that the intersection of the free-energy curves is not shifted by the quantum corrections to first order in the Wigner expansion,¹³ in contrast to the case of simple liquids.¹⁴ However, the volume change on melting is modified by quantum effects.

For the ions to be considered as essentially classical, the ratio of F^1/NkT over the classical free energy given by (2.10) must be very small; keeping only the dominant contribution in (2.10) (i.e., the purely static part of the free energy) this condition can be reexpressed as

$$(kT)_{\text{Ry}} \ll 14/\Gamma^2. \quad (3.5)$$

Combining (3.3) and (3.5) one sees that, in order for our model to be a reasonable approximation to dense ionized matter, one must verify the double condition

$$10 \gg (kT)_{\text{Ry}} \Gamma^2 \gg \frac{10^{-3}}{AZ^{2/3}}.$$

For He⁴ nuclei near the transition, $\Gamma_m = 158$, the model is reasonable if the temperature is in the range

$$10^{-3} \gg (kT)_{\text{Ry}} \gg 10^{-8}$$

or

$$2 \times 10^7 \text{ }^\circ\text{K} \gg T \gg 200 \text{ }^\circ\text{K}.$$

Choosing $(kT)_{\text{Ry}} = 10^{-1}/\Gamma_m^2$, the relative volume change $\delta v/v \simeq -3\delta\Gamma/\Gamma$, determined by the double-tangent construction, turns out to be exceedingly small, of the order of 0.03%. This value does not change very much with temperature. It is interesting to note that the relative volume change determined by Monte Carlo studies for various inverse-power potentials^{8,9,15} $1/r^n$ decreases with the exponent n . It is largest for hard spheres ($n = \infty$)¹⁶ (about 10%) and smallest in the Coulomb case ($n = 1$).

The entropy change of the ions on melting,

$$\frac{\delta S}{Nk} = \frac{\delta U}{NkT} - \frac{\delta F}{NkT},$$

is about 0.82, remarkably close to the values found for the various other inverse-power potentials.¹⁵ The "Lindemann ratio," i.e., the value of γ [formula (2.3)] at melting, is 0.17 for the 128-particle system, very close to the harmonic value of a system of that size.

The harmonic infinite system value is 0.165; this value will be adopted in the following sections. It should be noted that the Lindemann ratio for the ocp is somewhat larger than the one calculated for hard-sphere systems.¹⁰

As mentioned earlier, quantum corrections calculated to first order in the Wigner expansion do not shift the transition line in the $\rho - T$ plane. However, according to formula (3.4), quantum corrections *increase* with temperature along the classical melting line (characterized by a constant value of Γ), and at sufficiently high temperature we expect quantum effects to become so important that the Wigner \hbar^2 expansion ceases to be useful. In order to extend the phase diagram into the quantum region, we resort to lattice dynamics.

IV. LATTICE DYNAMICS OF ocp IN RIGID BACKGROUND

In this section we discuss some properties of the ocp solid with a uniform background within the framework of lattice dynamics. The principal new results given here are the equi- γ or Lindemann curves in the temperature-density planes. The Lindemann melting criterion identifies the solid-fluid coexistence curve with the equi- γ curve for the appropriate value of γ . Our choice of γ is determined from the Monte Carlo results in the classical region, as discussed in Sec. III. Previous harmonic calculations are commented on and

extended, and the application of the self-consistent phonon theory is discussed.

A Taylor-series expansion of the system potential energy in powers of the displacements of the lattice particles from their equilibrium sites leads, when truncated after the quadratic term, to the usual equations of the harmony theory¹⁷

$$\omega_j^2(\vec{q}) \vec{e}_j(\vec{q}) = \vec{D}(\vec{q}) \vec{e}_j(\vec{q}), \quad (4.1)$$

where the dynamical matrix D may be written in the form¹⁸

$$D_{\alpha\beta}(\vec{q}) = \omega_p^2 \left[\frac{\delta_{\alpha\beta}}{3} + \frac{f}{\pi} \sum_j \left(\frac{\delta_{\alpha\beta}}{n_j^3} - \frac{3n_j^\alpha n_j^\beta}{n_j^5} \right) e^{i\vec{q} \cdot \vec{R}_j} \right], \quad (4.2)$$

where the $n_j = (n_j^x, n_j^y, n_j^z)$ are integers, either all odd or all even for the bcc lattice or all even or two odd and one even for the fcc lattice. The factor f is 1 for the bcc case and $\frac{1}{2}$ for the fcc. This form shows explicitly that all density dependence is contained in the expression for the plasma frequency in this uniform background case. The dipolar sum in Eq. (4.2) may be evaluated by the Ewald method.¹⁹

The sum rule of Kohn follows from the form of the dynamical matrix as

$$\sum_j \omega_j^2(\vec{q}) = \sum_\alpha D_{\alpha\alpha}(\vec{q}) = \omega_p^2, \quad (4.3)$$

since the trace of the dipolar term is zero.

The initial attempts to accurately determine the first moment, giving the zero-point energy, were those of Coldwell-Horsfall and Maradudin²⁰ and of Carr.¹⁸ Carr calculated the frequencies exactly for a periodically repeated bcc lattice of 512 particles using a published tabulation of the necessary dipolar lattice sums¹⁹ to arrive at an answer of $U_1 = 0.511$. We have defined

$$U_n \equiv \left(\sum_{\vec{q}, j} \frac{\omega_j^n(\vec{q})}{\omega_p^n} \right) / (3N - 3), \quad (4.4)$$

where $3N - 3$ represents the vibrational degrees of freedom, the $\vec{q} = 0$ mode corresponding to center-of-mass motion being excluded. Coldwell-Horsfall and Maradudin tried to obtain the first moment from a knowledge of the first five even moments.²⁰ The last two of these are rather difficult to calculate and the moments they give can be shown to be mathematically inconsistent with a frequency distribution which is zero above the plasma frequency,²¹ this upper bound being easily seen from the Kohn sum rule. Explicit calculation shows their values of U_6 and U_8 to be about 10% too low. From our calculations, some results of which are given in Table II, we find the first moment for the infinite bcc lattice to be 0.511385.

In calculations of this kind the Kohn sum rule provides a convenient check for accuracy.

Among the lattice structures, hcp, bcc, fcc, and sc, the bcc is known to have the lowest static potential energy. We have calculated the free energy, in the harmonic approximation for the uniform background model, of the bcc and fcc phases and find the bcc phase to be increasingly the most stable phase at nonzero temperature. The vibrational free energy in the harmonic approximation, which is in addition to the static potential energy, is given by¹⁷

$$F = kT \sum_{\vec{q}, j} \ln \left[2 \sinh \left(\frac{\hbar \omega_j(\vec{q})}{2kT} \right) \right]. \quad (4.5)$$

This may be rewritten in terms of the dimensionless variable

$$\xi = [\gamma_s^{3/2} (kT)_{Ry}]^{-1} \quad (4.6)$$

as

$$F(\xi) = kT \sum_{\vec{q}, j} \ln \{ 2 \sinh [\sqrt{3} \xi \omega_j(\vec{q}) / \omega_p] \}. \quad (4.7)$$

For large values of ξ this becomes

$$F(\xi) = (3N - 3)kT \sqrt{3} U_1 \xi. \quad (4.8)$$

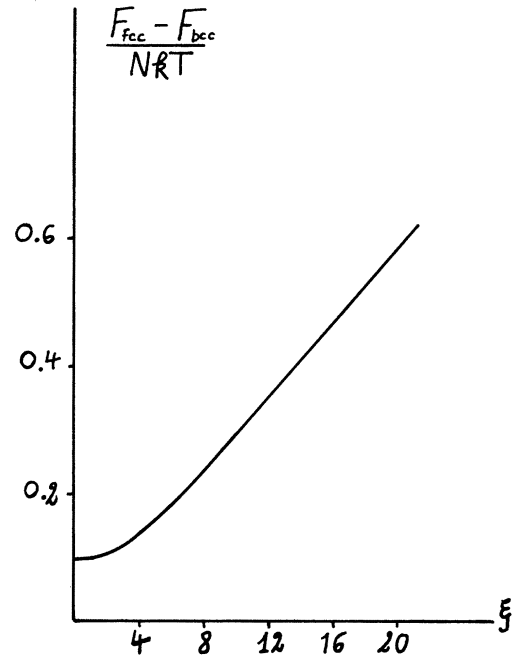


FIG. 1. Difference between the vibrational free energies of the fcc and bcc phases for the ocp with uniform background. The calculation is for a harmonic lattice of $(36)^3$ particles or 139 965 internal degrees of freedom. The bcc is predicted as the stable phase for all values of the parameter ξ [defined by formula (4.6)].

Figure 1 shows the calculated difference in vibrational free energy between the bcc and fcc phase. Table IV gives our values for the vibrational free energy and specific heat of the bcc phase.

The mean-squared displacement is calculated from the expression¹⁷

$$\langle U^2(O) \rangle = \frac{\hbar}{(2N-2M)} \times \sum_{\vec{q}, j} \frac{\coth\left[\frac{1}{2}\left[\frac{\beta\hbar}{\omega_j(\vec{q})}\right]\right]}{\omega_j(\vec{q})}. \quad (4.9)$$

We divide this by the square of the nearest-neighbor distance to obtain an expression for γ^2 as defined previously in Eq. (2.3). The reader is warned that this ratio has been defined by other writers as the mean-squared displacement divided by the Wigner-Seitz radius \bar{r} .^{4,22} For the bcc lattice, to which we restrict ourselves hence, this ratio is

$$\gamma^2 = \frac{1}{2(3r_s)^{1/2}} \left(\frac{3}{\pi}\right)^{2/3} \frac{1}{3N-3} \times \sum_{\vec{q}, j} \frac{\coth\left[\sqrt{3}\xi\omega_j(\vec{q})/\omega_p\right]}{\omega_j(\vec{q})/\omega_p}. \quad (4.10)$$

This has two convenient limiting forms:

$$\gamma^2 \sim \frac{1}{2(3r_s)^{1/2}} \left(\frac{3}{\pi}\right)^{2/3} U_{-1}, \quad \xi \gg 1 \quad (4.11)$$

$$\gamma^2 \sim \frac{r_s}{6} \left(\frac{3}{\pi}\right)^{2/3} (kT)_{Ry} U_{-2}, \quad \xi \ll 1. \quad (4.12)$$

The large- ξ limit defines the quantum region and the small- ξ limit the classical region. From (4.11) we have calculated the equi- γ or Lindemann curves for several values of γ close to the one given at melting by the Monte Carlo studies. These are shown in Fig. 2. A previous estimate based on a Debye model fitted to the moments of Ref. 20 was given in Ref. 5 for the case $\gamma=0.17$. The general form for the curves of Fig. 2 may be seen from Eqs. (4.11) and (4.12). We shall use r_0 to denote the value of r_s for melting at $T=0^\circ$. The curves of Fig. 2 clearly show the strong dependence of the zero-temperature melting density on γ ($r_0 \sim \gamma^{-4}$) and also the sensitivity of the maximum melting temperature. The essential improvement here over previous estimates of r_0 based on the Lindemann criterion is the determination of a "reasonable choice" of γ from "exact" Monte Carlo computer studies on the same system in the classical region. As mentioned above, the value of γ at melting is predicted to be 0.16–0.17.

Our value of γ at melting is somewhat larger than the value 0.15 estimated by Van Horn⁴ for the alkali metals and used to predict a value of

$\Gamma=170$ for melting in the classical region. Nozières and Pines²² use a value of γ only slightly smaller than that of Van Horn; however, their estimate of the inverse first moment [see Eq. (4.11)] is inadequate. They neglect the transverse branches completely and consider only a dispersionless longitudinal branch. It is, however, the lower-frequency predominantly transverse branches which are most important for an inverse moment. They effectively estimate U_{-1} as $\frac{1}{3}$, whereas the correct value is close to 2.8. Since U_{-1} is squared in calculating r_0 their estimate differs considerably from ours. Their choice of γ with the correct value of U_{-1} would give a value of r_0 close to 1500, rather than the 20 which they estimated and which has been often quoted. The large value of r_0 somewhat weakens the appeal of using low-density electron-solid results for purposes of interpolation into the range of metallic densities.

In concluding this section we discuss efforts to apply self-consistent harmonic theory to the uniform-background model.

The self-consistent phonon (SCP) theory has been applied to this system by Kugler²³ and the

TABLE IV. Vibrational free energy and specific heat per particle for the ocp lattice in the uniform-background model. The independent variable ξ used here is defined in Eq. (4.7) of the text.

ξ	$\frac{F}{kT}(\xi)$	$\frac{C_v}{3k}$
0.1	-5.6692	0.996 68
0.2	-3.5748	0.986 86
0.3	-2.3336	0.970 95
0.4	-1.4361	0.949 62
0.5	-7.228	0.923 66
0.6	-0.1227	0.894 01
0.7	0.401 66	0.861 60
0.8	0.8726	0.827 35
0.9	1.3045	0.792 09
1.0	1.7067	0.756 53
1.5	3.4558	0.590 63
2.0	4.9890	0.460 33
2.5	6.4306	0.362 96
3.0	7.8268	0.289 29
3.5	9.1982	0.232 45
4.0	10.555	0.188 01
4.5	11.903	0.152 98
5.0	13.245	0.125 18
5.5	14.583	0.103 01
6.0	15.918	0.085 23
6.5	17.252	0.070 91
7.0	18.585	0.059 30
7.5	19.916	0.049 86
8.0	21.247	0.042 14
8.5	22.578	0.035 80
9.0	23.908	0.030 56

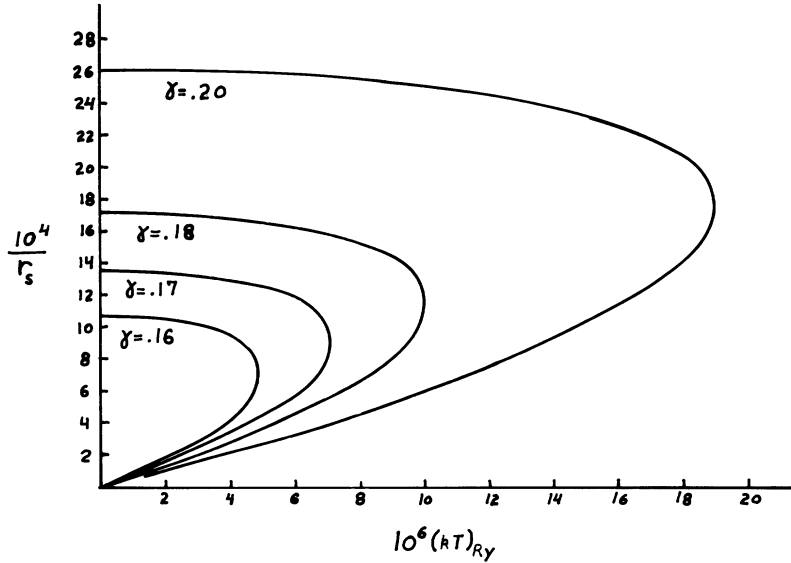


FIG. 2. Equidisplacement or Lindemann curves as a function of density and temperature for several values of γ close to the value given by the Monte Carlo studies as appropriate for melting in the classical regime. The parameter is defined as the rms displacement divided by the nearest-neighbor distance. The calculations are for a harmonic lattice of $(36)^3$ particles and a uniform background.

reader is referred to this paper for a very thorough discussion. The density dependence of the system is now no longer given solely by that of the plasma frequency. Kugler has tabulated some of the frequency moments of this system as a function of r_s for the zero-temperature case. For r_s less than about 50 these differ noticeably from the harmonic values and, in fact, for r_s less than about 22, no self-consistent solution was found. For the largest r_s tabulated, however ($r_s = 90.5$), they converge quite well to the harmonic results. The first moment here, for example, differs by about 0.2% from the harmonic value.

We have checked Kugler's results for the zero-temperature case and find them completely accurate. In extending them to nonzero temperatures we find that the "lattice instability" noticed by Kugler persists. For example, at $r_s = 50$ there is no solution to the SCP equations for temperatures above about 0.9×10^{-3} Ry/ k and at $r_s = 2 \times 10^4$ above 0.32×10^{-5} Ry/ k . These values are, however, far outside the region of stability of the solid phase and are of no significance quantitatively. In the region where we have predicted the solid phase as stable, the solutions of the SCP equations are essentially identical to the harmonic-theory results. The computer experiments show that the anharmonic contribution to the internal energy (as mentioned before) is quite small but clearly larger than the statistical uncertainty in the results. The lowest-order SCP theory shows a deviation from harmonicity several orders of magnitude smaller than this.

Kugler has extended the theory to include the "second-order" cubic term and has presented a very approximate calculation showing that at zero

temperature the dispersion curves even for r_s as large as 800 do in fact differ from the harmonic results. We plan to check to determine if this difference is present in the classical region by molecular-dynamics studies now underway.

V. LATTICE DYNAMICS OF ocp IN RESPONSIVE BACKGROUND

In this section we shall examine in a semiquantitative way the effects on the Lindemann curves of allowing the charge-neutralizing background to respond to the motion of the lattice particles. Recall that the model which we have in mind is that of nuclei in an electron-gas background. The possible astrophysical significance of this model has been discussed by Ruderman.²⁴ The conclusion we arrive at is that, for α particles and heavier nuclei (the heaviest we consider here is iron), the screening by the background does not radically change the Lindemann curves from the uniform-background case. Only a lattice of protons and, to some extent, of deuterons requires a consideration of screening.

We assume, as is physically reasonable, that the electrons react instantaneously, on a time scale of the vibrational period of the nuclei, so that we may describe this response using the static dielectric function for the background system. From electrostatics the induced charge is related to the "external charge," here the nuclei, by

$$\rho_{\text{ind}}(\vec{q}) = \left(\frac{1}{\epsilon(\vec{q})} - 1 \right) \rho_{\text{nuc}}(\vec{q}), \quad (5.1)$$

where

$$\rho_{\text{nuc}}(\vec{q}) = \frac{Ze}{V} \sum_i e^{i\vec{q}\cdot\vec{r}_i} \quad (5.2)$$

and V is the system volume. From Poisson's equation the electrostatic potential is

$$\Phi(\vec{q}) = \frac{4\pi}{q^2} \frac{\rho_{\text{nuc}}(\vec{q})}{\epsilon(q)}, \quad (5.3)$$

and, looking at the potential energy of a lattice particle, one sees that

$$\phi(r) = \frac{4\pi Z^2 e^2}{V} \sum_{\vec{q}} \frac{e^{i\vec{q}\cdot\vec{r}}}{q^2 \epsilon(q)} \quad (5.4)$$

may be regarded as the effective pair potential between the nuclei. If this is used in the standard equation for the dynamical matrix

$$D_{\alpha\beta}(\vec{q}) = \frac{1}{M} \sum_{n \neq 0} \nabla_{\alpha} \nabla_{\beta} \phi(r) \Big|_{r=R_n} \times (1 - e^{-i\vec{q}\cdot\vec{R}_n}), \quad (5.5)$$

we obtain

$$D_{\alpha\beta}(\vec{q}) = \omega_p^2 \sum_G \left(\frac{(\vec{G} + \vec{q})_{\alpha} (\vec{G} + \vec{q})_{\beta}}{(\vec{G} + \vec{q})^2 \epsilon(\vec{G} + \vec{q})} - \frac{G_{\alpha} G_{\beta}}{G^2 \epsilon(G)} \right), \quad (5.6)$$

where the \vec{G} are reciprocal-lattice vectors resulting from the sum over equilibrium lattice sites in Eq. (5.5). The dynamical matrix can be rewritten in another form as

$$D_{\alpha\beta}(\vec{q}) = D_{\alpha\beta}^C(\vec{q}) + \omega_p^2 \sum_G \left[\frac{(\vec{G} + \vec{q})_{\alpha} (\vec{G} + \vec{q})_{\beta}}{(\vec{G} + \vec{q})^2} \left(\frac{1}{\epsilon(\vec{G} + \vec{q})} - 1 \right) - \frac{\vec{G}_{\alpha} \vec{G}_{\beta}}{G^2} \left(\frac{1}{\epsilon(G)} - 1 \right) \right], \quad (5.7)$$

where D^C is the dynamical matrix for the uniform-background case, Eq. (4.2).

The density and temperature ranges we are interested in are of the same order as for the uniform-background case. Since our distance unit is the Bohr radius of the lattice particles, for protons or heavier particles it is necessary to consider a very-high-density electron-gas background. Comparing the Fermi momentum to $m_e c$ we have

$$\frac{\hbar k_F}{m_e c} = \left(\frac{e^2}{\hbar C} \right) \left(\frac{m_u}{m_e} \right) \left(\frac{9\pi}{4} \right)^{1/3} \frac{AZ^{7/3}}{r_s} \approx 25.5 \frac{AZ^{7/3}}{r_s}, \quad (5.8)$$

where m_u is the unit atom mass. The r_s range we shall examine extends to values less than 1000 where this ratio, even for α particles, is of order

1, so in this region the electron gas must be treated relativistically.

Except for protons and deuterons the Fermi temperature is greater than 10^3 times the temperature for almost all r_s and T we consider, so in this case it is possible to use a dielectric function calculated for a degenerate electron gas.

For the sake of convenience and also because it demonstrates the basic ideas we have used the Fermi-Thomas dielectric function. This has the form

$$\epsilon(q) = 1 + k_{FT}^2 / q^2, \quad (5.9)$$

with²⁵

$$k_{FT} = k_{FT}^{\text{nonrel}} \left[\left(\frac{\hbar k_F}{mC} \right)^2 + 1 \right]. \quad (5.10)$$

We shall mention below where it may be anticipated that this overly simple dielectric function will be wrong. Using (5.9) in (5.4) the effective pair potential is

$$\phi(r) = Z^2 e^2 (e^{-k_{FT} r} / r). \quad (5.11)$$

For a bcc lattice the ratio of nearest-neighbor distance d to the screening length k_{FT}^{-1} is

$$k_{FT} d = \sqrt{3} (36\pi)^{1/6} \left(\frac{e^2}{\hbar C} \right) Z^{1/3} \left[1 + \left(\frac{mC}{\hbar k_F} \right)^2 \right]^{1/4} \approx 0.325 Z^{1/3} \left[1 + \left(\frac{r_s}{25.5 A Z^{7/3}} \right)^2 \right]^{1/4}. \quad (5.12)$$

If we are to approach the uniform-background results this ratio should be less than 1. As Z increases the minimum value of this ratio, obtained at $r_s = 0$, increases rather slowly; however, what is more important is the rapid increase of $A Z^{7/3}$ so that $k_{FT} d$ for values of A and Z corresponding to α particles or heavier nuclei stays near its minimum value until r_s is well into the low-density classical regime. This will be seen more clearly from the numerical results presented below.

The dynamical matrix derived from (5.11) is easily found to be

$$D_{\alpha\beta}(\vec{q}) = \omega_p^2 \left(\frac{k_{FT}^3}{4\pi\rho} \right) \left\{ \frac{\delta_{\alpha\beta}}{3} \sum_{j \neq 0} \frac{e^{-x_j}}{x_j} + \sum_{j \neq 0} \left[\delta_{\alpha\beta} \left(\frac{1}{x_j} + \frac{1}{x_j^2} \right) - x_j^{\alpha} x_j^{\beta} \left(1 + \frac{3}{x_j} + \frac{3}{x_j^2} \right) \right] \frac{e^{-x_j}}{x_j} \times e^{-i\vec{x}_j \cdot \vec{q}/k_{FT}} \right\}, \quad (5.13)$$

with $X_j \equiv R_j k_{FT}$. It is interesting to compare the

dispersion curves obtained from this dynamical matrix for various values of r_s with those of the uniform-background model. We have taken $A = Z = 1$ and \bar{q} along [100] to make this comparison in Fig. 3 for two values of r_s . Referring to Fig. 3 we see that for the smaller r_s , and thus $k_F r_d$, we approach the uniform-background result with the transverse branch only slightly changed and the longitudinal branch close to the uniform-background result except near the origin. In these units a density corresponding to, say, metallic sodium at zero pressure would correspond to r_s of order 8000. In this case the curves would be almost an order of magnitude below the uniform-background results. On the other hand, it is known from neutron-scattering experiments that in the alkali metals the transverse branch along [100], for example, is only slightly changed from the uniform-background case.²⁶ In general, the model would estimate the screening effects as far more important than they actually are in this case. As this model has in the past been used to discuss phonons in metals (see Ref. 27 for a discussion of some of these calculations), we will comment further on this.

If the problem of phonons in metals is studied using a local pseudopotential, a dynamical matrix

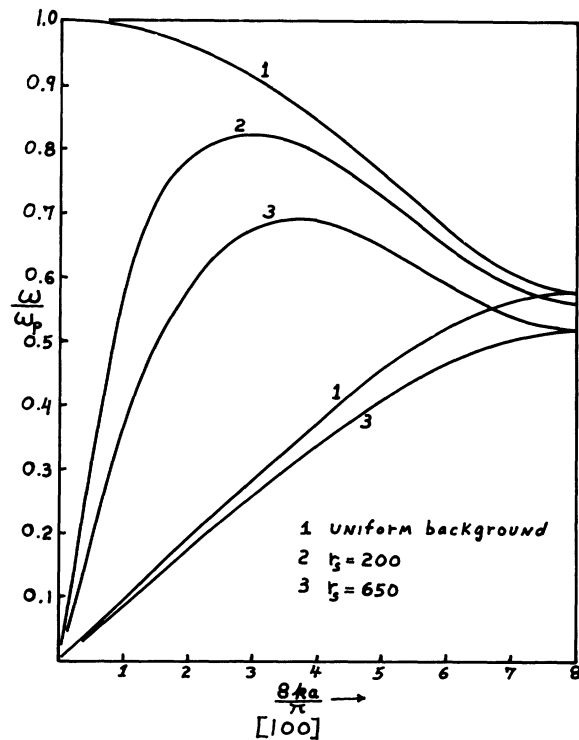


FIG. 3. Comparison of the dispersion curves along (100) of the uniform-background case with those for the case of a responding background with Fermi-Thomas screening. The results are for $A = Z = 1$.

of the form of Eq. (5.7) may be derived, with the difference that in the sum over reciprocal-lattice vectors the bracketed terms containing the dielectric function are multiplied by essentially the square of the quantity, Fourier transform of the pseudopotential times the square of the wave vector [see Ref. 28, Eqs. (2.3.4) and (2.3.5)]. In noting the difference between this and the model shown in Fig. 3 it is convenient to use a form of the pseudopotential due to Ashcroft which is Coulomb-like outside some core radius r_c and zero for $r < r_c$.²⁹ The zero results from a cancellation between the Coulomb potential within the core and the kinetic energy resulting from the orthogonalization of the conduction-electron wave function to the core wave functions. The parameter r_c is adjustable to allow for the fact that this cancellation is not complete. For this pseudopotential the dynamical matrix is given by Eq. (5.7) with the terms containing the dielectric function multiplied by the square of the cosine of the quantity r_c times the wave vector [see Ref. 30, Eqs. (3), (5), and (7)]. With an r_c appropriate to sodium, for example, the neutron data are well fitted by the calculated dispersion curves, with some small dependence on the dielectric used; in particular, except for the term in the dynamical matrix [Eq. (3.7)] corresponding to $G = 0$, the results are not considerably changed from the uniform-background case. However, these results are quite sensitive to the value of r_c and by reducing this value the terms due to screening become more important. This is well illustrated in Fig. 5 of Ref. 30 for a 4% decrease in r_c , and we have checked this rapid increase in the importance of screening for larger decreases in r_c . It is the neglect of the importance of the ion core in reducing screening effects which causes the model shown in Fig. 3 to be even qualitatively incorrect as a model for phonons in metals with an ion core. Our results are therefore confined to a lattice of fully ionized atoms.

We have recalculated the Lindemann curves using the potential (5.11) for the particular case $\gamma = 0.17$, which was roughly the value given at melting by the Monte Carlo studies of the uniform-background model. The results are shown in Fig. 4. As the curves for the nuclei heavier than, say, the deuteron are close to the uniform-background results, it is likely that this value of γ may approximately describe melting in this more general case. For the proton and deuteron lattice this value is probably incorrect, but from our studies to date we cannot say more about this.

Since we are studying the rms displacement which depends primarily on the low-frequency long-wavelength modes, we might hope that the Fermi-Thomas dielectric which is correct in the

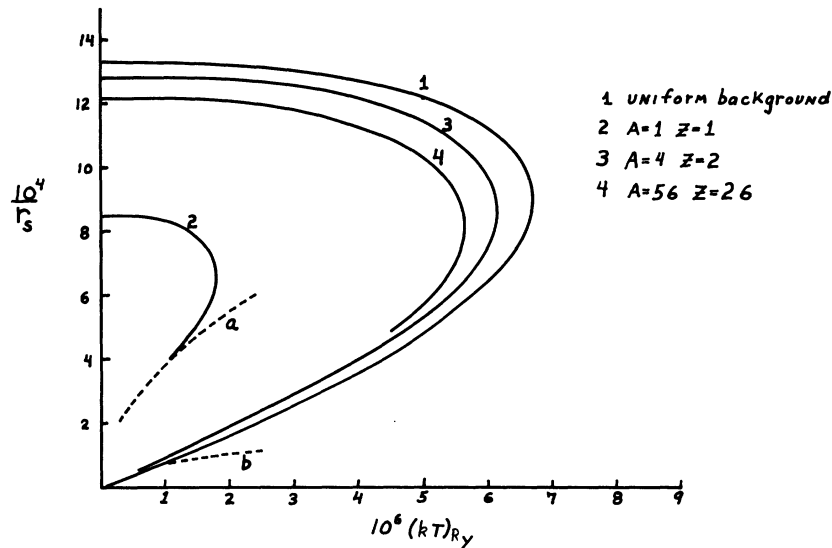


FIG. 4. Comparison of the Lindemann curves for $\gamma=0.17$ between the uniform-background case and the case of a responding background with Fermi-Thomas screening for a few values of A and Z as indicated. A harmonic lattice of $(8)^3$ particles was used here. With the exception of $A=Z=1$, the curves are quite close. For $A=Z=1$ the screening effects are quite large and a more thorough study with a more realistic choice of dielectric function would be needed for quantitative conclusions. The dashed lines a and b indicate some values of density and temperature, where the ratio of the Fermi temperature to system temperature is 10^{+3} for $A=Z=1$ and for $A=4, Z=2$, respectively. The curve for $A=56, Z=26$ has not been continued into the low-density region for visual clarity.

long-wavelength limit would be a good approximation. This is probably true, for the most part, except that from Eq. (5.6) it is necessary to note that the dielectric function will also enter as $\epsilon(\vec{G}+\vec{q})$ for $G \neq 0$. When the screening and therefore the terms with $G \neq 0$ become most important, it is expected that a form for the dielectric function accurate at large q values would give better results. Stated somewhat differently, it is well known that the exponential decay in the potential predicted by the Fermi-Thomas dielectric is not the correct asymptotic form, which corresponds instead to Friedel oscillations.³¹ Therefore, if the screening length is so short that even nearest neighbors may be in the asymptotic region of the potential, it is likely that results based on the Thomas-Fermi form are wrong. This applies strongly to the proton and deuteron lattices, but for the heavier nuclei studied would be important only at quite low densities.

VI. CONCLUSION

In this paper we have presented the results of a study of the crystalline phase of the one-component plasma. We believe this system to be important not only in itself, as the low-density limit of the electron gas, for example, and as a possible astrophysical model, but also as a limiting case in the systematic study of purely repulsive in-

verse-power potentials where the hard-sphere system is the other limiting case. We list here what we believe to be the most important results.

(a) A value of the melting parameter $\Gamma_m = 155 \pm 10$ was obtained for the system in the classical region. The value of the Lindemann parameter leads, in conjunction with conventional lattice dynamics, to an estimate of $r_0 \approx 800$ for melting at $T=0^\circ$ in the quantum regime.

(b) For melting in the classical region the entropy change of the ions, $\delta S/Nk \approx 0.82$, is quite close to values obtained for all other inverse-power potentials, including hard spheres. The relative volume change on melting, $\delta V/V \sim 0.03\%$, is however, considerably smaller than for other repulsive inverse-power potentials.

(c) A preliminary investigation of the effect of allowing the background to respond to the ionic motion indicates that the melting curves given by the Lindemann criterion are probably unchanged for $Z \geq 2$. The case of ions with $Z=1$ is inconclusive.

Future work will concentrate on the time-dependent properties and a more accurate treatment of dielectric screening.

ACKNOWLEDGMENTS

One of us (E. L. P.) wishes to thank the Institut National des Sciences Techniques Nucléaires

(France) for the grant of a Joliot-Curie fellowship. We are indebted to B. Jancovici for many helpful discussions and a very thorough and critical reading of the manuscript. One of us (J. P. H.) acknowledges stimulating conversations with B. J. Alder.

APPENDIX

As we have discussed above, the Monte Carlo results show the anharmonicity of the solid ocp to be quite small but undeniably present. The anharmonicity increases the internal energy and appears to be proportional to the square of temperature. This contrasts with computer studies on the r^{-12} potential where the internal energy is lowered from its harmonic value by a term proportional to the temperature. The basic cause of this difference can be understood from a simple cell model, although it is not sufficient for numerical comparison, as it gives too small a value for the rms displacement.

In the cell model a particle is assumed to move in the field of its neighbor particles, which are taken to be at their equilibrium positions. For the solid ocp the derivation of the potential proceeds as usual (we take the system volume as large but finite for the moment). The potential seen by a particle is then

$$V(r) = V_{\text{static}} + e^2 \sum_{l \neq 0} \left(\frac{1}{|\bar{\Gamma} - \bar{\Gamma}|} - \frac{1}{|\bar{\Gamma}|} \right) - \rho e^2 \int d^3r' \left(\frac{1}{|\bar{\Gamma}' - \bar{\Gamma}|} - \frac{1}{r'} \right), \quad (\text{A1})$$

where r is the distance of the particle from its equilibrium position. The second term is expanded in spherical harmonics.

$$e^2 \sum_{l \neq 0} \left(\frac{1}{|\bar{\Gamma} - \bar{\Gamma}|} - \frac{1}{|\bar{\Gamma}|} \right) = 4\pi e^2 \sum_{j=1}^{\infty} \sum_{m=-j}^j \frac{r^j}{2j+1} Y_{jm}(\Omega_r) \sum_{l \neq 0} \frac{Y_{lm}(\Omega_l)}{l^{j+1}}. \quad (\text{A2})$$

By the usual arguments of crystal-field theory we note (i) if the crystal has inversion symmetry then only terms for even j are nonzero. (ii) For a cubic crystal the polar axis may be taken along an axis of fourfold symmetry so that only terms with $m=0, \pm 4, \pm 8, \dots$ are nonzero. (iii) For a cubic crystal the term in Y_{20} is explicitly zero. (iv) Since the potential is real the coefficients of Y_{jm} and Y_{j-m} are equal.

We may finally write

$$\beta V = \beta V_{\text{static}} + \frac{\Gamma}{2} x^2 + 4\pi\Gamma \sum_{j=4}^{\infty} \frac{x^j}{2j+1} \times \left(D_{j0} Y_{j0}(\Omega_x) + \sum_{m=4,8,\dots} D_{jm} [Y_{jm}(\Omega_x) + Y_{jm}^*(\Omega_x)] \right), \quad (\text{A3})$$

where $x = r/\bar{r}$ and

$$D_{jm} = \bar{r}^{j+1} \sum_{l \neq 0} \frac{Y_{lm}(\Omega_l)}{l^{j+1}},$$

with

$$\Gamma \equiv e^2 \beta / \bar{r}, \quad \beta = 1/kT$$

and we may take infinite-system limit.

The essential difference between this expression and what is obtained for any other power-law potential is that here the quadratic term is the only isotropic part of the potential.

We now treat the terms beyond the quadratic as a perturbation and do classical thermodynamic perturbation theory:

$$\beta F = \beta F_0 + \langle \beta V_{\text{pert}} \rangle_0 - \frac{1}{2} (\langle \beta^2 V_{\text{pert}}^2 \rangle_0 - \langle \beta V_{\text{pert}} \rangle_0^2) + O(\beta^3). \quad (\text{A4})$$

The term $\langle \beta V_{\text{pert}} \rangle_0$ is zero since the perturbation contains no isotropic part and

$$\langle \beta^2 V_{\text{pert}}^2 \rangle_0 = (4\pi)^2 \Gamma^2 \sum_{j=4}^{\infty} \frac{1}{(2j+1)^2} \times \left(\langle x^{2j} Y_{j0}^2 \rangle_0 D_{j0}^2 + \sum_{m=4,8,\dots} D_{jm}^2 \langle x^{2j} [Y_{jm} + Y_{jm}^*]^2 \rangle_0 \right). \quad (\text{A5})$$

The necessary averages are

$$\langle x^{2l} Y_{l0}^2 \rangle_0 = \frac{1}{\pi} \left(\frac{2}{\Gamma} \right)^l \left(\frac{(2l+1)!!}{2^{l+2}} \right), \quad (\text{A6})$$

$$\langle x^{2l} [Y_{lm} + Y_{lm}^*]^2 \rangle_0 = \frac{2}{\pi} \left(\frac{2}{\Gamma} \right)^l \left(\frac{(2l+1)!!}{2^{l+2}} \right).$$

So we have

$$\beta F = \beta F_0 - 2\pi \sum_{j=4}^{\infty} \frac{(2j+1)!!}{(2j+1)^2} \left(\frac{1}{\Gamma} \right)^{j-2} \times \left(D_{j0}^2 + 2 \sum_{m=4,8,\dots}^j D_{jm}^2 \right). \quad (\text{A7})$$

The internal energy is obtained from

$$U = \frac{\partial}{\partial \Gamma} (F\Gamma), \quad (\text{A8})$$

which verifies that the internal energy is increased from a harmonic result by a leading term proportional to the temperature squared.

If we repeat the argument for some other power-law potential, then the isotropic term is no longer purely quadratic but contains terms in x^4 , x^6 , etc.

If the quadratic term is again taken as the reference potential, the first-order perturbation term is now nonzero, since the perturbing potential contains isotropic parts. The leading x^4 term now gives the correct sign and temperature dependence noted in the r^{-12} studies. It appears that the solid ocp is a rather special case in this regard.

The D coefficients appearing in (A7) may be

evaluated from the standard lattice sum tabulations.³² As mentioned above, the numerical value given by (A7) for the Γ^{-2} term is too small, since (A3) gives too small an rms displacement. It is possible to play numerical games and multiply the quadratic in (A3) by a factor chosen so that the reference Einstein oscillator has the same rms displacement as given by the harmonic theory in the classical limit, and then the Γ^{-2} coefficient in (A7) has an order-of-magnitude agreement with the computer results.

*Joliot-Curie Fellow.

†Laboratoire associé au Centre National de la Recherche Scientifique. Postal address: Bât. 211, Université de Paris-Sud, 91 Orsay, France.

¹J. P. Hansen, preceding paper, Phys. Rev. A 8, 3096 (1973).

²N. A. Metropolis, A. W. Rosenbluth, M. N. Rosenbluth, A. H. Teller, and E. Teller, J. Chem. Phys. 21, 1087 (1953).

³S. G. Brush, H. L. Sahlin, and E. Teller, J. Chem. Phys. 45, 2102 (1966).

⁴H. M. Van Horn, Phys. Lett. A 28, 706 (1969).

⁵J. P. Hansen, B. Jancovici, and D. Schiff, Phys. Rev. Lett. 29, 991 (1972).

⁶J. P. Hansen, Phys. Lett. A 41, 213 (1972).

⁷F. C. Von der Lage and H. A. Bethe, Phys. Rev. 71, 612 (1947).

⁸J. P. Hansen, Phys. Rev. A 2, 221 (1970).

⁹W. G. Hoover, M. Ross, K. W. Johnson, D. Henderson, J. A. Barker, and B. C. Brown, J. Chem. Phys. 52, 4931 (1970).

¹⁰D. Young and B. J. Alder (unpublished).

¹¹R. W. Zwanzig, J. Chem. Phys. 22, 1420 (1954).

¹²F. J. Dyson and A. Lenard, J. Math. Phys. 8, 423 (1967); A. Lenard and F. J. Dyson, J. Math. Phys. 9, 698 (1968).

¹³E. Wigner, Phys. Rev. 40, 749 (1932).

¹⁴J. P. Hansen and J. J. Weis, Phys. Rev. 188, 314 (1969).

¹⁵W. G. Hoover, S. G. Gray, and K. W. Johnson, J. Chem. Phys. 55, 1128 (1971).

¹⁶B. J. Alder and T. E. Wainwright, Phys. Rev. 127, 539 (1962); W. G. Hoover and F. H. Ree, J. Chem. Phys. 49, 3609 (1968).

¹⁷A. Maradudin, E. W. Montroll, and G. H. Weiss, *Theory of Lattice Dynamics in the Harmonic Approximation* (Academic, New York, 1963).

¹⁸W. J. Carr, Jr., Phys. Rev. 122, 1437 (1961).

¹⁹M. H. Cohen and F. Keffer, Phys. Rev. 99, 1128 (1955).

²⁰R. A. Coldwell-Horsfall and A. A. Maradudin, J. Math. Phys. 1, 395 (1960).

²¹J. C. Wheeler and R. G. Gordon in *The Padé Approximant in Theoretical Physics*, edited by G. A. Baker, Jr. and J. L. Gammel (Academic, New York, 1970).

²²P. Nozières and D. Pines, Phys. Rev. 111, 442 (1958).

²³A. E. Kugler, Ann. Phys. 53, 133 (1969).

²⁴M. Ruderman, J. Phys. (Paris) 30, C3-152 (1969).

²⁵B. Jancovici, Nuovo Cimento 25, 428 (1962).

²⁶R. A. Cowley, A. D. B. Woods, and G. Dolling, Phys. Rev. 150, 487 (1966).

²⁷S. K. Joshi and A. K. Rajagopal, Solid State Phys. 22, 160 (1968).

²⁸L. J. Sham, Proc. R. Soc. Lond. A 283, 33 (1965).

²⁹N. W. Ashcroft, J. Phys. C 1, 232 (1968).

³⁰D. L. Price, K. S. Singwi, and M. P. Tosi, Phys. Rev. B 2, 2983 (1970).

³¹J. S. Langer and S. H. Vosko, J. Phys. Chem. Solids 12, 196 (1960).

³²D. C. Wallace and J. L. Patrick, Phys. Rev. 137, A152 (1965).